



Supplementary Materials for

Measles virus infection diminishes preexisting antibodies that offer protection from other pathogens

Michael J. Mina[†], Tomasz Kula, Yumei Leng, Mamie Li, Rory D. de Vries, Mikael Knip, Heli Siljander Marian Rewers, David F. Choy, Mark S. Wilson, H. Benjamin Larman, Ashley N. Nelson, Diane E. Griffin, Rik L. de Swart, Stephen J. Elledge[†]

[†]Corresponding author. Email: selledge@genetics.med.harvard.edu (S.J.E.);
mmina@hsph.harvard.edu (M.J.M.)

Published 1 November 2019, *Science* **366**, 599 (2019)
DOI: 10.1126/science.aay6485

This PDF file includes:

Materials and Methods
Figs. S1 to S12
Table S1
References

Materials and Methods

Samples

Clinical measles specimens and specimens from MV uninfected cohort: An observational cohort study was performed during a measles outbreak in the Orthodox Protestant community in the Netherlands (24). Unvaccinated children aged four to 17 years old at the moment of sampling, without a history of natural measles, were recruited by distributing invitation letters and patient information forms via three Orthodox Protestant schools with low vaccination coverage. Clinical specimens were collected after verbal assent was obtained from participants younger than 12 years old or written informed consent from participants aged 12 years and older. Written informed consent from both parents was always obtained. Plasma samples were collected, heat-inactivated (30 minutes, 56C), clarified (15 min, 1000g) and stored at -20C. The study protocol was approved by the medical ethical committee of Erasmus MC, the Netherlands (MEC-2013-302, CCMO register NL45323.078.13/2).

Control samples used: Control specimens for control cohorts A, B, C and MMR vaccinated controls were obtained as secondary use research specimens and came from healthy controls who were sampled longitudinally for prior research efforts. The MMR vaccinated controls were derived from healthy children in the long-term DIABIMMUNE birth cohort study (43). Control samples for Cohort C were derived from serum stored from a collection of otherwise healthy adults with asthma. Childhood control samples were derived from healthy children enrolled in the DAISY prospective study of children with increased risk for Type 1 Diabetes, recruited between 1993 and 2004, with followup through 2018 (44). For each of the control specimens, all ethical approvals were met for the original study purposes and for follow-up studies and are detailed in each of the references noted.

Macaque infection experiments: Three-year old male rhesus macaques from the Johns Hopkins primate breeding facility were infected intratracheally with 10^4 plaque-forming units of the Bilthoven strain of wild type measles virus and heparinized blood samples were obtained from ketamin-anesthetized animals as previously described (34). All studies were performed in accordance with experimental protocols approved by the Johns Hopkins University Institutional Animal Care and Use Committee.

Virscan 2.0 Construction

For the present study, we constructed an extended VirScan library – VirScan 2.0. The VirScan 2.0 library was generated by supplementing the original VirScan library with additional viral and non-viral antigens. All proteins from the following viral species were identified in the UniProt database, collapsed on 90% identity, and bioinformatically parsed into 56 amino-acid peptide sequences with 28 amino-acid overlaps between adjacent tiles:

Adeno-associated virus: (UniProt taxonomy ID 1511891); Cosavirus A: 1330491; GB virus; C/Hepatitis G virus: 54290; Human torovirus: 67605; MERS coronavirus: 1335626; Merkel cell; polyomavirus: 493803; Oropouche virus: 118655; Rosavirus A: 1511805; Salivirus A: 1330524; Zika virus: 64320; Cercopithecus erythrotis polyomavirus: 1236395; Convict Creek 107 virus: 37705; FinV707 virus: 1204159; Madariaga virus: 1440170; Saimiriine herpesvirus: 10381; Ebolavirus: 186536; Chikungunya virus: 37124; Lassavirus: 11620; SV40: 10633

To select the most relevant non-viral antigens to include in the VirScan 2.0 library, all reported antigens from the Immune Epitope Database (IEDB; (45)) were filtered to exclude human, viral,

and malarial proteins. The full-length proteins of the remaining 571 antigens were extracted from UniProt and bioinformatically parsed into 56 amino-acid peptide sequences with 28 amino-acid overlap.

Oligonucleotides corresponding to the original VirScan library and additional antigens were programmed into Agilent microarrays, and were then amplified and ligated into bacteriophage T7 DNA, packaged into phage particles and amplified in *E. coli* to form the VirScan phage library at a density of 1.5×10^{11} pfu/ml as previously described (25). The VirScan 2.0 library contained a total of 115,753 peptides. Approximately 2×10^{10} pfu ($\sim 1.5 \times 10^5$ pfu representation of each epitope) are combined with 2 μ g of sample IgG ($\sim 0.2 \mu$ L of serum or plasma), and following an overnight incubation at 4° C antibody bound phage are immunoprecipitated and balanced amplicon libraries are pooled and sequenced. The read counts per peptide are converted to a relative antibody epitope binding signal (EBS) and magnitude reported as epitope specific Z-scores.

Calculations for epitope binding signal (EBS) Z-scores and detection of antibody hits

For every epitope in VirScan, we calculate enrichment Z-scores to determine epitope ‘hits’ (i.e. presence of an antibody to a particular epitope) and to quantify the relative magnitude of enrichment for each epitope – referred to as the epitope binding signal (EBS) in the main text. We used a slight modification to the original VirScan statistical pipeline (25), detailed below.

The VirScan library, like any phage display library, is comprised of a distribution of phage abundances. This means that some peptides are displayed at higher numbers than others. To best compare like against like, we created statistical bins of comparable peptides. By ‘comparable’, we mean peptides that derive from the same ‘slice’ of the distribution and thus

have uniform abundance (determined by NGS read counts per peptide in control VirScan samples). To create bins comprising peptides with uniform abundance, peptides (i.e. specific phage clones) were first ranked-ordered.

Rank order peptides: To determine rank, we summed the epitope-specific NGS read counts (after normalization to 1 million reads each) obtained from between 4-10 ‘beads-only’ controls (i.e. VirScan performed without adding any blood sample) and ordered the epitopes based on these sums. Epitope position after ordering defined the rank, and ties assumed the same rank.

Creation of bins with uniform baseline epitope abundance: Next, bins were created by first binning epitopes with identical ranks and then, if the bin contained fewer than 300 epitopes, additional epitopes with adjacent ranks were added until each bin contained at minimum 300 epitopes. VirScan 2.0 contains approximately 115,000 epitopes and it was therefore common for > 300 epitopes to be tied for the same exact rank (fig. M1).

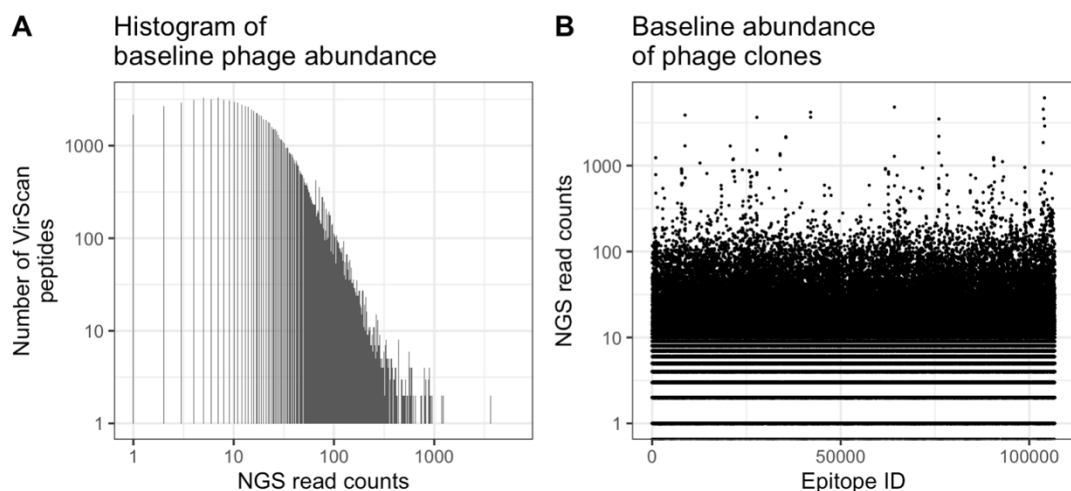


Figure M1. Beads-only VirScan runs were performed in the absence of any serum/plasma or other antibody containing sample. The NGS read counts for each epitope in the beads-only samples are shown as a histogram in (A). In (B) the same data is plotted as a scatter plot with the NGS read counts for each epitope (y-axis) plotted against the VirScan epitope ID (an arbitrary ID number assigned to every epitope in VirScan). A and B demonstrate the expected distribution of phage at baseline across the library.

Choice of minimum bin size: We found that 300 epitopes per bin i) allowed for robust statistical and enrichment calculations when applied to the actual sample counts while ii) being sufficiently narrow to ensure that each bin is comprised only of phage with identical or very similar baseline abundance (fig M2), ensuring that all epitopes had ‘equal opportunity’ for determination of enrichment when applied to the actual samples. Sensitivity analysis of the bin size demonstrated that the particular size has no effect on any statistical calculations as long as the target size was between approximately 30 and 1000 epitopes (below 30 led to occasional stochastic fluctuations and above 1000 could undermine the assumption that the phage included in each bin were of similar baseline abundance). The exception was when > 1000 epitopes were all tied with the same rank. In these cases, there was no limit on the allowable bin size as identically ranked epitopes by definition have identical expected baseline abundance.

Calculation of Z-scores: Once the epitopes to be included in each bin were determined, the actual values of the beads-only runs were no longer required, and only the list of epitope identifiers destined for each bin was carried forward to the actual sample analysis.

For each sample, the NGS read counts for each epitope were grouped into their now predefined bins. For each bin, the top and bottom 5% of epitopes by NGS counts were temporarily removed, and the middle 90% used to obtain mean and standard deviation required for Z-score calculations. Because we expect that only between 0.5% - 2% of all epitopes in VirScan will be targeted by antibodies in any particular blood sample, these middle 90% of epitopes in each bin serve as appropriate null distributions from which to calculate Z scores.

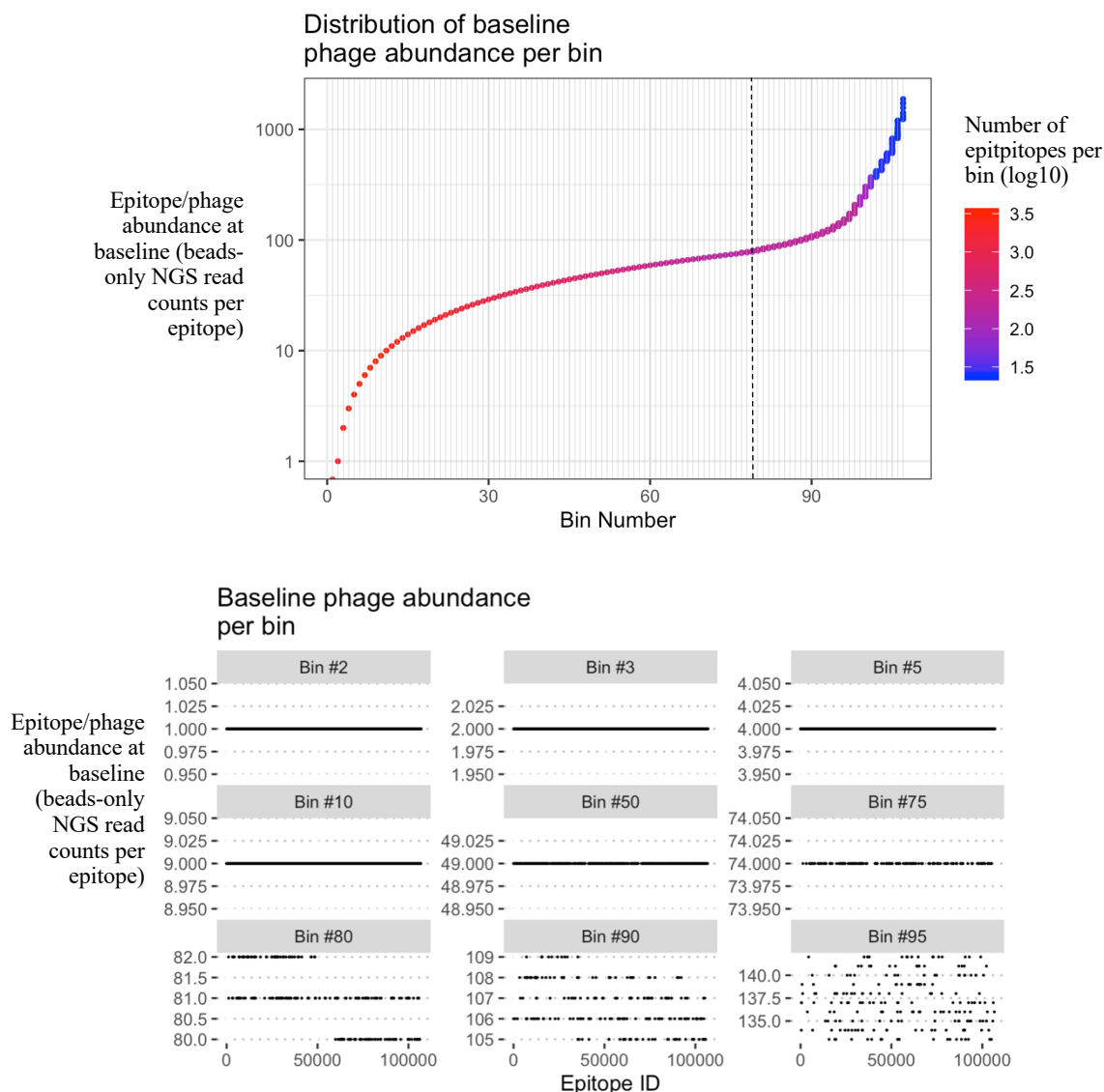


Figure M2. Example distribution of bins for a VirScan library. (Top) Each point indicates the relative abundance of epitopes (y-axis) in each bin (x-axis), and the number of epitopes with that abundance (color). For many bins (all bins before the vertical dashed line), all epitopes included per bin have identical abundance / rank (i.e. ties based on NGS read counts from the beads-only runs). Thus, in the top panel, the color indicates the number of epitopes with each rank (points) in each bin. (Bottom) Examples of the baseline abundance of each epitope in a selection of bins from the top panel. For example, bin #50 contains ~500 distinct peptides (shown by the color in the top panel), which are binned together because they all have the identical or similar relative abundance (NGS read counts of 49 in this example) and derive from different pathogens from across the entire VirScan library (exemplified by the inclusion of epitopes from across the spectrum (x-axis) of unique epitope identifiers). In the bottom panel, ‘Epitope ID’ is the unique epitope identifier given to each distinct epitope, and is not a quantitative value.

For Z-score calculations, for the j^{th} bin, the mean (μ_j) and standard deviations (σ_j) of the NGS read counts of the middle 90% of epitopes were calculated and a Z-score for each epitope (i) in bin (j) was obtained as: $Z_{ij} = (counts_{ij} - \mu_j) / \sigma_j$

where $counts_{ij}$ is the NGS read counts for the i^{th} epitope in the j^{th} bin. The process was then repeated for every bin and for every sample.

Testing robustness of Z-scores calculated within bins by comparing against a distinct Z-score methodology

By comparing each epitope in a sample to other ‘like’ epitopes from the same sample (i.e. comparing epitopes in the same bin of the same sample), this approach (‘Method 1’) benefits from automatically controlling for assay or batch-specific effects. An alternative approach (‘Method 2’) is one akin to many RNA-seq approaches: i) each sample is run alongside a series of controls, ii) NGS counts are normalized to obtain equal total reads in each sample and controls, and iii) enrichment of each epitope is calculated directly by comparison against the control NGS counts for that epitope (i.e. fold-enrichment or Z-score). Thus in this alternative approach, the controls are used as direct comparisons rather than strictly for binning. Such an approach is slightly more intuitive because it directly quantifies enrichment of an epitope in a sample by comparing against the same epitope in serum-free controls. However, that approach places heavy reliance on a relatively small number of data points (i.e. 8 controls means 8 data points are used for calculating each epitope’s null distribution: mean and standard deviation). In contrast, the binning approach we employ here estimates the null distribution from at least $n = 300$ epitopes with an expected equal abundance (based on controls) and from the same sample. The alternative (method 2) approach additionally requires that a new set of at least eight controls is run each time a new set of samples are run – a resource intensive requirement. Because

calculating enrichments relative to controls is standard practice in many applications, we tested the robustness of the binning method by comparing the two approaches and found nearly identical results (Fig. M3), demonstrating that the null distributions derived per bin from the middle 90% within-sample epitope read counts are appropriate distributions for calculation of Z-score enrichments and hits. An additional method which lies between the two approaches just described has also been considered (see Yuan et al. BioRxiv, April 26, 2018. DOI 10.1101/2855916) and performs similarly (not shown).

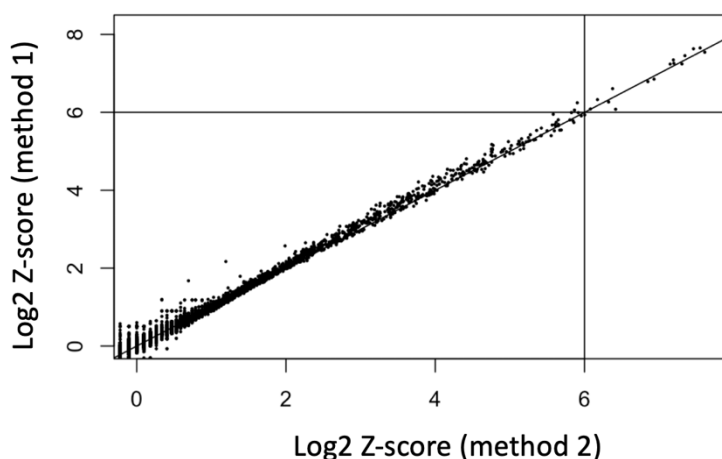


Figure M3. Comparison of calculated Z-scores using two different methods. Y-axis: Z-scores were calculated based on Method 1: binning epitopes as described above and used in the main-text. X-axis: Z-scores were calculated based on Method 2: direct comparison of normalized NGS read counts per epitope in the sample against the mean and standard deviation for each epitope measured across 8 control VirScan runs.

Determining antibody-epitope hits

Presence of antibody against a particular epitope in patient sera is determined when, upon immunoprecipitation an epitope has a Z-score > 3.5 standard units in at least two separate technical replicates (Figure M4). To maximize sensitivity of VirScan, when serial samples exist (i.e. multiple samples taken from the same individual at at least two different points in time), we leverage the added confidence in detection that comes from multiple samplings. Thus, to

maximize sensitivity, when an epitope is recognized in using the conventional threshold of 3.5 in two technical replicates (just described), then for other time points within the serial sampling we relax the required threshold and apply a Z-score threshold of >2 units in at least two replicate samples for a particular epitope. Again, this is only for specific epitopes that are detected at a different time point from the same individual using the more conservative thresholds. The end result is that, for each sample, we obtain a binary response for whether a particular peptide was recognized (an antibody epitope “hit”), and we also can obtain a value for the antibody epitope binding signal (EBS) strength, taken as the mean of the two (or more, if >2 replicates were performed) replicates. The binning procedure used for calculating Z-scores leads a desirable uniform distribution of hits and EBS across all levels of the library regardless of baseline phage abundance.

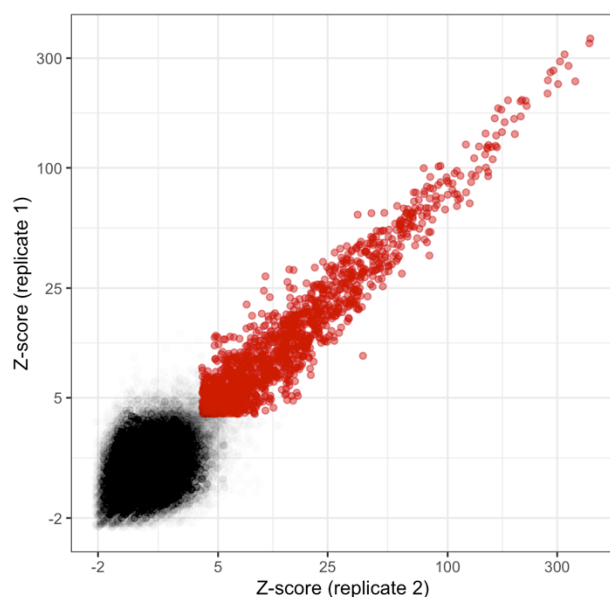


Figure M4. Determination of epitope hits. Antibodies are considered to be present when a Z-score above 3.5 is detected in two distinct sample replicates. Shown above is a representative sample. Each axis represents the Z scores (placed on a log-scale) of two replicates drawn from the same sample. Each point indicates a single epitope in VirScan. Significant hits (i.e. epitopes considered to be enriched by presence of sample antibody) are shown in red.

Observing that Z-scores are quantitative

To demonstrate that Z-scores as described above are appropriate quantitative metrics for measuring antibodies in plasma (versus simply presence/absence), we ran VirScan on plasma at 1x and 0.1x dilutions (Fig. M5). Two representative examples are shown. As expected, the median Z-score across all of the epitopes for which an antibody hit was detected is essentially 10-fold-higher in the 1x versus the 0.1x dilution (Left panel: Median fold-change across epitopes is 10.4 [IQR 6.88 – 18.1]; Right panel: 11.7 [IQR 7.4 – 20.1]). This shows that VirScan Z-scores (EBS) calculated via the binning methods accurately capture quantitative antibody values akin to ELISA antibody titers.

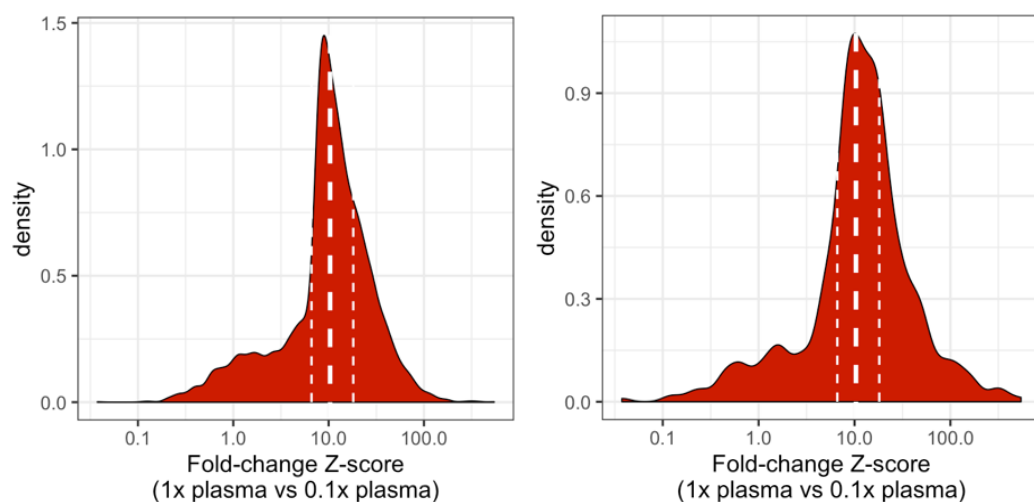


Figure M5. VirScan Z-scores accurately quantify antibodies in plasma. Two representative examples of VirScan runs performed with 1x plasma and 0.1x plasma on two samples are shown (left and right). For each, Z-scores were calculated for each epitope, as above, and the fold-change Z-score in the 1x versus the 0.1x dilutions were calculated and density distributions of those fold-changes are shown here. Median and interquartile ranges are drawn for each.

Cross-reactive antibody epitope hits

Antibody cross-reactivity is common across pathogens. This is particularly notable when, for instance, antibody hits are repeatably observed in a given individual for pathogen epitopes for

which no exposure to the pathogen should have occurred (i.e. VirScan routinely picks up cross-reactive antibodies that bind to MERS, HIV, and Ebola virus peptides). When using VirScan for serological surveillance or prevalence studies, among other uses, pathogen-specific thresholds are applied. For example, a simple criteria might include a minimum number of epitope hits for a given pathogen that must be achieved to consider a pathogen exposure to have occurred. The application of these thresholds, determined separately for each pathogen, ensure that results are specific. For the current study however, because the overall aim was to understand the changes in the numbers and levels of antibodies across the repertoire after measles, in order to obtain the best estimate of overall change, all detected antibodies considered to be true biological hits were considered regardless of whether they represented on-target or cross-reactive antibodies.

ELISA measurement of antiviral antibody titers

Paired pre/post sera from 20 patients (15 measles cases, 5 controls) were tested in duplicate for IgG concentrations against Enterovirus (QED Biosciences, ESR133G), Adenovirus (QED Biosciences, ESR128G), and Respiratory syncytial virus (QED Biosciences, ESR113G) according to manufacturer's protocol.

Random effects model for estimating probability of antibody retention per pathogen

A random effects model was used to estimate probability of antibody retention per pathogen per individual, while controlling for sampling interval, set to 3 months. The model response variable was antibody presence as a binary attribute (1/0). Fixed effects included cohort (MV mild, MV severe, MV negative, and Control A combined with Control B were the reference group). The random effect was modeled with pathogen species nested within the individual from whom the

paired sample was drawn. For some of the controls, multiple paired samples were drawn from a single individual. The model structure was:

Ab present (0/1) ~ cohort + interval + random(1|individual/species) (family = "binomial").

The model was run using the *glmer* function set with a *bobyqa* optimizer within the R package *lme4 v1.1*. The per pathogen probabilities of antibody retention were obtained using the *response* output of the *predict.merMod* (defined within *lme4 v1.1*) function.

Data analysis

All Statistical methods are as described throughout the main text and in the methods above. All statistical analyses and figures were produced using R (Version 3.5.2; R core team, Vienna, Austria. 2018) and benefitted from working within the RStudio integrated development environment. Packages used include: *parallel*, *data.table*, *nlme*, *lme4*, *forcats*, *dplyr*, *ggplot2*, *ggpubr*, and *future.apply*.

Cohort^a	N^b	Age^c, years mean (sd)	Interval^d, weeks mean (sd)
Control A (age & interval matched paired specimens)	28	7.4 (2.8)	15.6 (5.2)
Control B (age matched paired specimens)	31	9.8 (2.6)	52.0 (10.4)
Control C (interval matched adult paired specimens)	22	49.7 (11.7)	5.2 (5.2)
Measles Uninfected paired specimens	5	9.1 (1.9)	13 (5.2)
MMR Vaccinated paired specimens	33	1.7 (0.3)	26 (2.8)
Measles mild paired specimens	34	9.1 (1.9)	10.4 (5.2)
Measles severe paired specimens	43	9.4 (2.0)	10.4 (5.2)
Rhesus macaques paired specimens	4	3 (0.0)	22 (0.0)

Table S1: Description of cohort and specimens used in this study

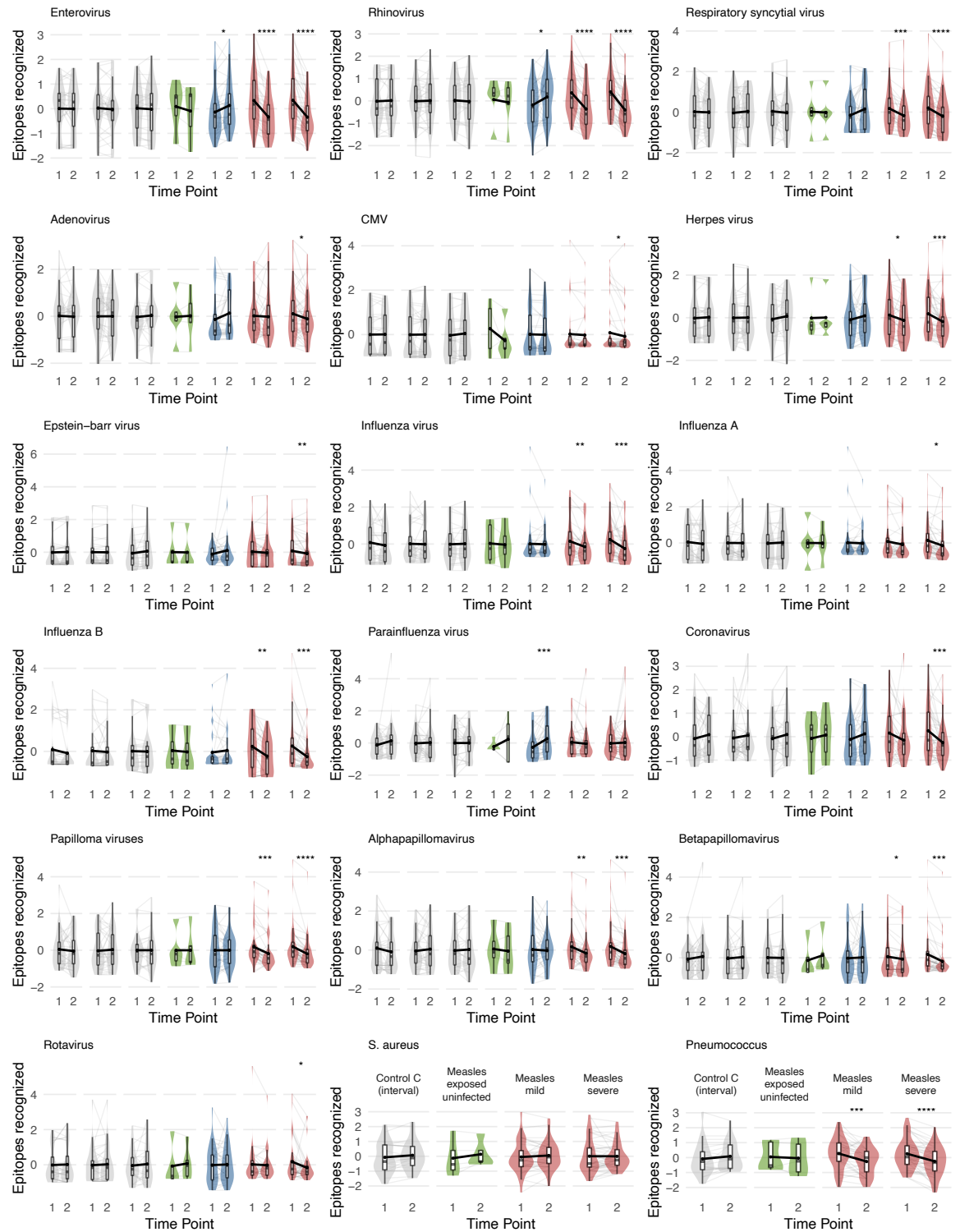
^a Cohort referred to in study

^b Number of paired specimens obtained per cohort

^c Age at time of initial sample

^d Duration of time (weeks) between specimen collections

Figure S1. Measles eliminates antibody diversity. The standardized (mean = 0, SD = 1) epitopes recognized per individual for 18 of the most commonly recognized pathogens are shown. Violin plots show the distributions at each time point of the number of epitopes recognized across the children per cohort. Each individual is indicated by a thin gray line connecting the two time points and the averages between the two time points per cohort are connected by a dark black line.



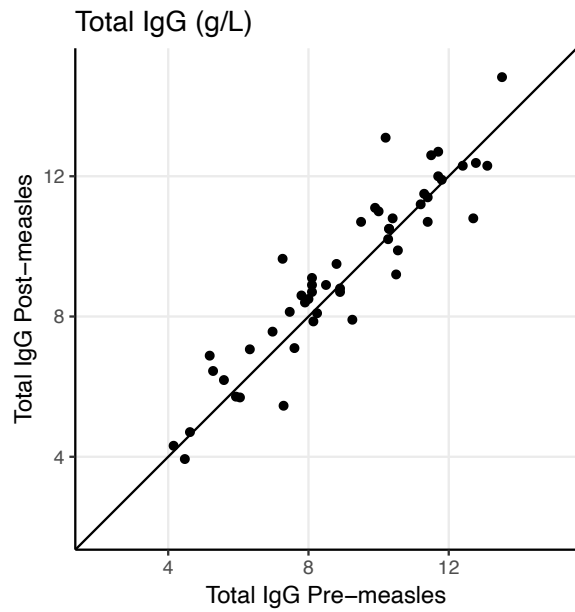


Figure S2. Total ELISA IgG titers are unchanged after measles. Total IgG titers were measured using commercially available total IgG ELISA quantitative assays for a selection of 50 of the 77 children before and after measles infection. Each point represents total IgG before (x-axis) and after (y-axis) measles infections. Overall, total IgG levels remained essentially unchanged after measles and the mean IgG concentration was approximately 9 g/L. Total IgA and IgM levels also were unchanged and are reported in Ref. 24.

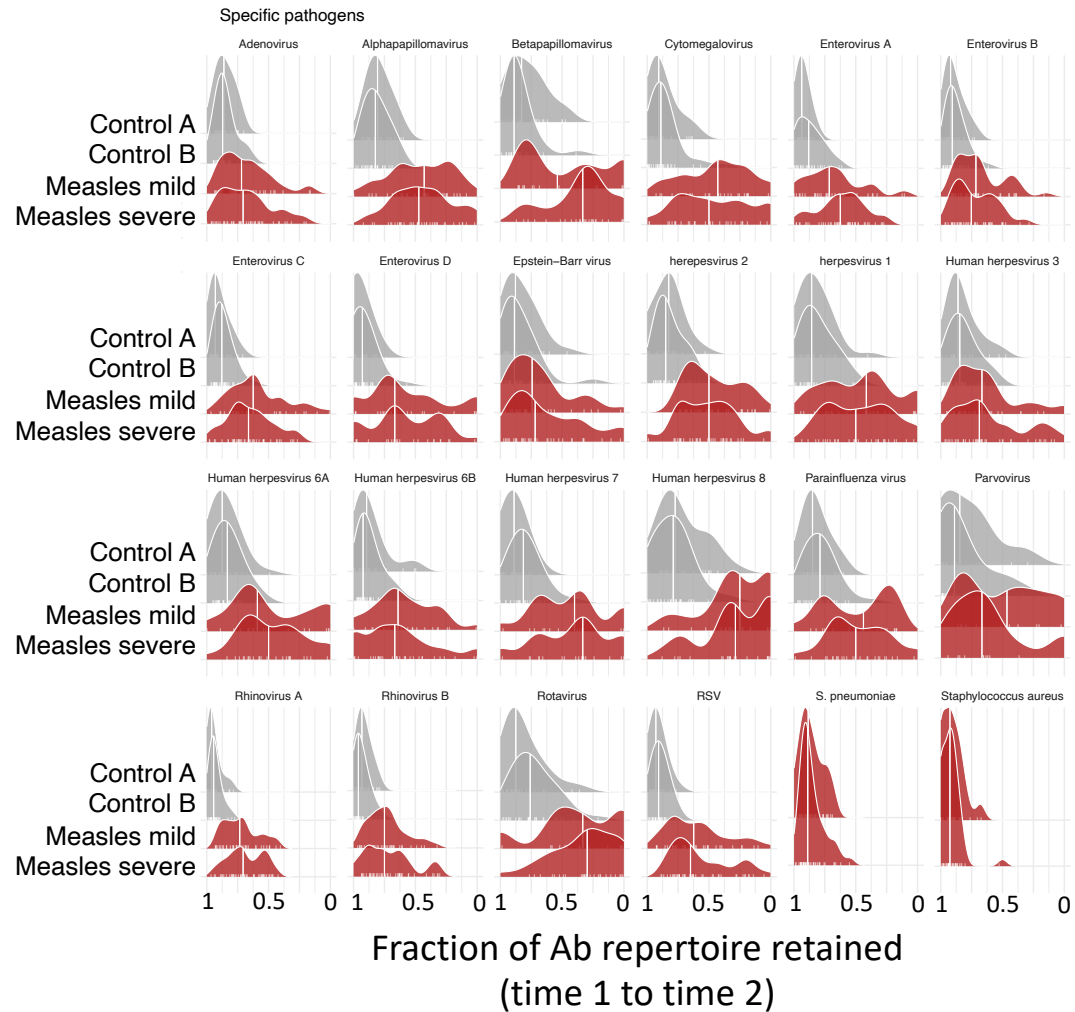
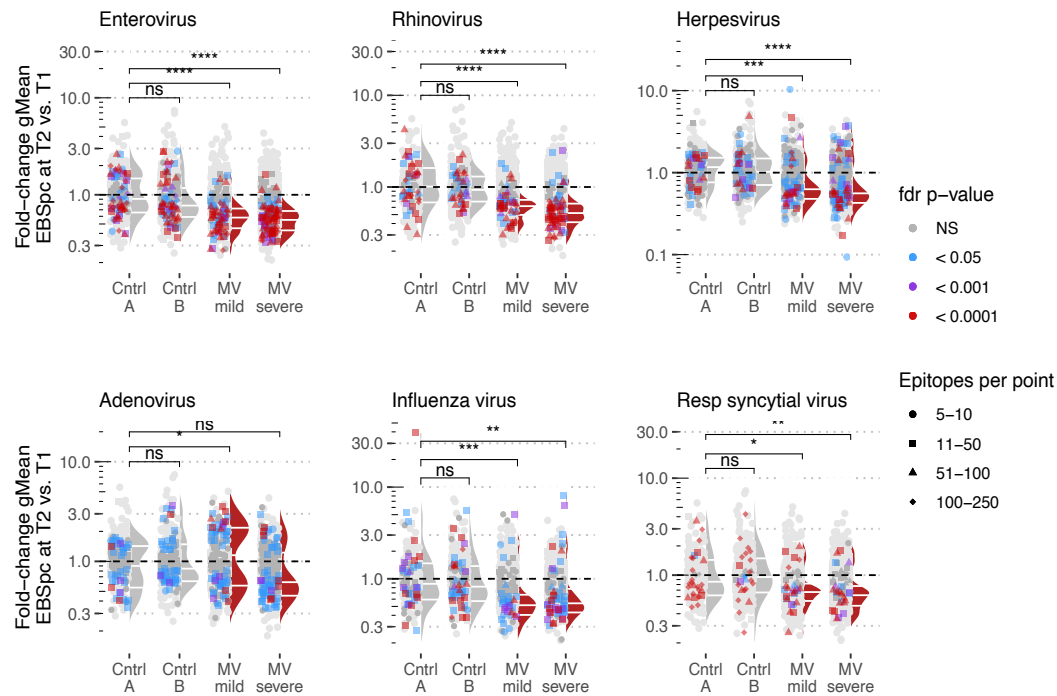


Figure S3. Proportion of epitopes retained from time 1 to time 2. Shown are density plots representing the fraction of the pathogen specific antibody repertoires retained across children in each cohort.

The measles uninfected control cohort is shown in Figure 2 but is removed from individual pathogen plots due to small sample sizes ($n = 5$ individuals total in this cohort).

In each plot, a value of one (x-axis) indicates no loss of the antibody repertoire over the sampling interval and zero indicates complete loss. Each white tick mark indicates one individual.



*For all panels, one point includes analysis of all epitopes from one pathogen per child

Figure S4 Measles virus infections are associated with diminished epitope binding signal for specific pathogen-associated epitopes. Data are as presented in Figure 3A, but here broken out by representative pathogens. In each panel, a single point represents one pathogen species per child from within the named pathogen family (i.e. enterovirus, rhinovirus, herpesvirus, etc...). Multiple strains are included for each pathogen family and combined here for visualization and statistical purposes (i.e. Influenza consists of both Influenza A and B). EBS for all epitopes recognized for each pathogen species per individual were compared using a Wilcoxon matched-pairs signed rank test, and fdr adjusted p-values (adjusted to obtain a false discovery rate of 5%) are indicated by color of each symbol. The total number of epitopes included in each paired test (i.e. the number of epitopes recognized for each species per child) are indicated by the symbol shape. For each pathogen and child combination, the geometric mean (gMean) EBS was calculated at each time point and the fold-change at time 2 versus 1 was calculated and indicated by the position of each point along the y-axis. Density distributions adjacent to the points reflect the distribution of points that were significantly changed based on an fdr p-value > 0.05.

**Measles virus
infected
(N = 15)**

**Measles
virus
exposed &
uninfected
(N = 5)**

Fold-change in binding signal (EBS)
(VirScan) or titers (ELISA) at Time 2 vs. 1

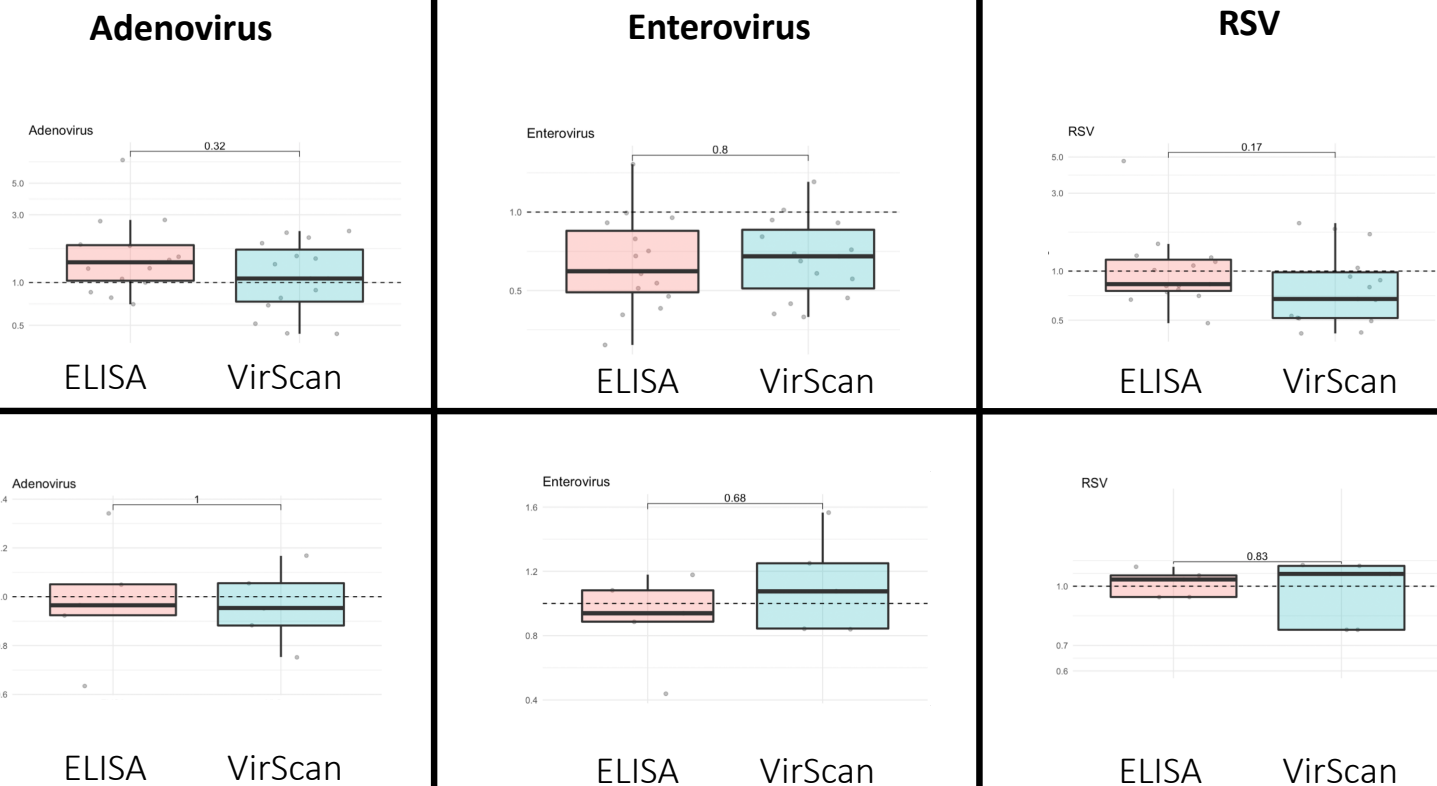


Figure S5a. VirScan results agree with traditional ELISA assay results. Samples from 20 individuals were selected from among the 77 measles infected cohort, and each of the 5 measles exposed but uninfected cohort. In order to confirm VirScan results that were detected in both directions (i.e. positive and negative overall changes after measles) the 15 samples from the measles cohort were selected to include individuals who had both increases or decreases in geometric mean antibody epitope binding signals (EBS) for adenoviruses and RSV, and one individual with a positive increase in overall EBS for enteroviruses. Therefore, the overall effects noted here are not representative of the overall effects described in the main text as this comparison was to compare relative changes measured by ELISA compared to VirScan. Because the commercial ELISA assays were ‘general’ and include proteins from numerous strains (though details are not provided by the manufacturer), for this comparison we calculated the geometric mean EBS for *all* epitopes in VirScan for each of the three virus classes (adenovirus, enterovirus, and respiratory syncytial virus) that each individual recognized at each time point, and plotted the ratio of these means. Assay results between ELISA and VirScan were compared using a paired t-test (paired per individual). Results for measles infected (upper) and measles uninfected (lower) are plotted.

Despite the major differences in the two methodologies, no significant differences were noted among any of the comparisons. Of note, it is possible that the RSV and Adenovirus ELISA assays may have increased sensitivity to new infections because unlike VirScan, the ELISAs capture antibodies to conformational and linear epitopes (whereas VirScan detects primarily linear or secondarily folded epitopes only). The tradeoff is that while an ELISA provides a single titer value – an average of all antibodies that bind – VirScan provides individual EBS strengths for antibodies to each individual epitope.

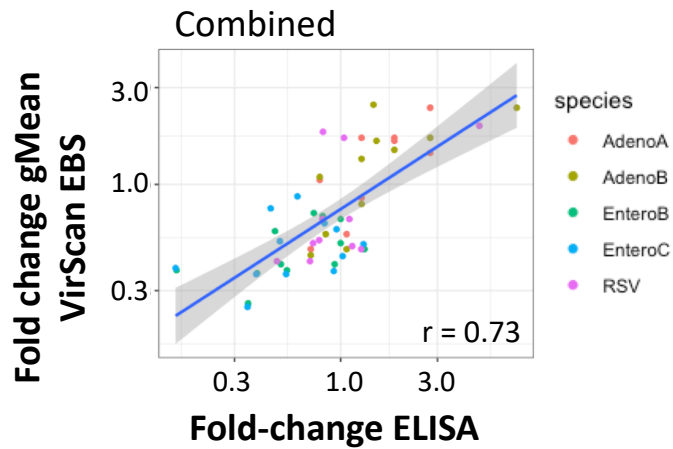
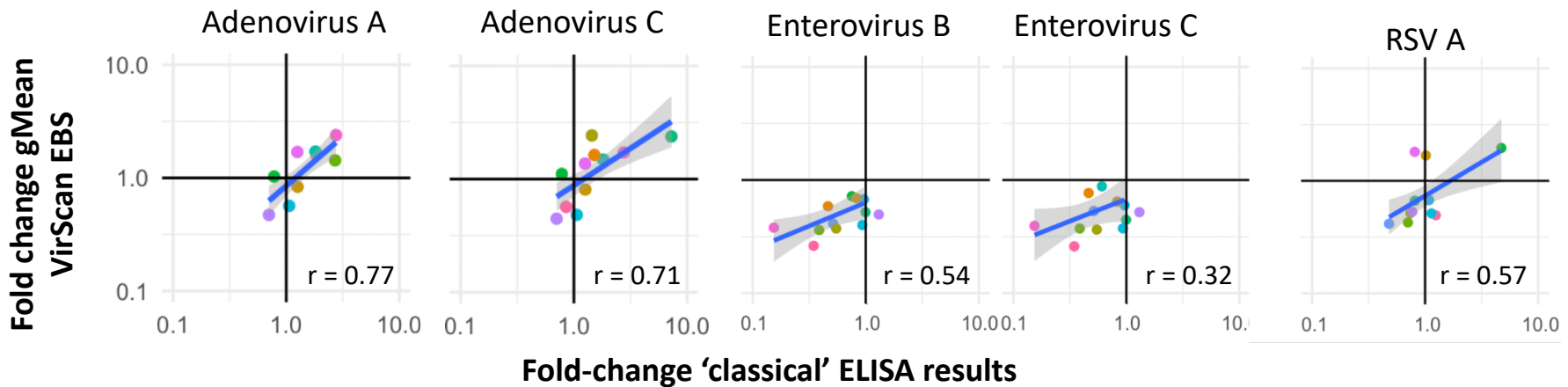


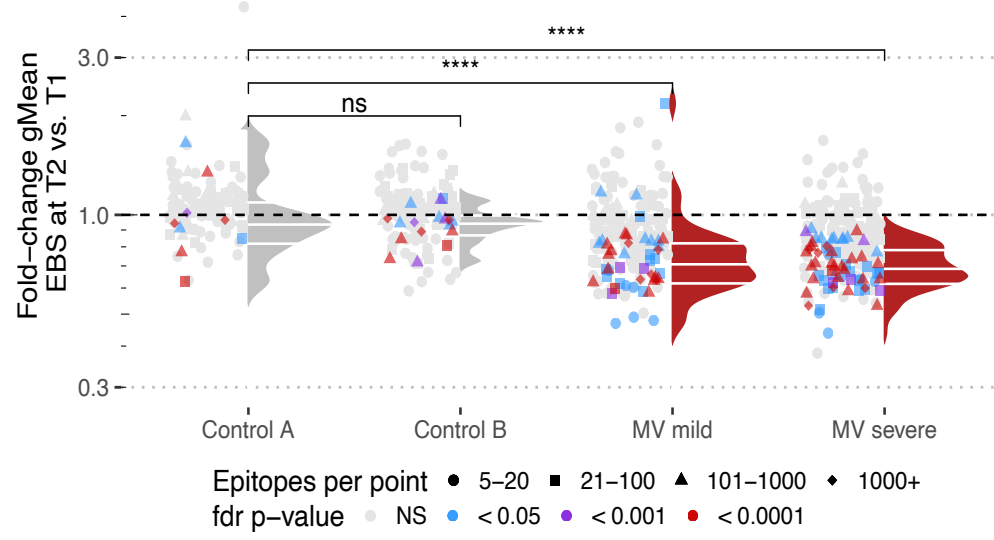
Figure S5b. VirScan EBS compared to traditional ELISA assays. Samples from a subset of measles infected individuals were run using 'classical' adenovirus, enterovirus and respiratory syncytial virus ELISA assays. These assays each contain whole pathogen reagents, including numerous species for each pathogen family.

Y-axis fold-change in the geometric mean antibody Epitope Binding Signal (EBS) for the indicated pathogen per child at time 2 versus 1.

X-axis fold-change in adenovirus (left two panels), enterovirus (middle two) or RSV (right-most panel) ELISAs at time 2 versus 1.

Though major differences in technologies, the assay results indicate strong concordance. For example, because ELISAs provide an aggregate measurement of all antibodies that bind any epitope on the included viruses, ELISA results can be driven up by even a single high titer antibody. VirScan on the other hand is epitope specific and when averaged across all epitopes based on geometric means, it should not be driven up by any single antibody, even if that antibody is very high titer.





One point = one pathogen species across all children per cohort

Figure S6. Change in EBS per pathogen species per cohort. The change in the geometric mean EBS for all epitopes within a pathogen species across all children per cohort was measured. Each point represents one pathogen species per cohort, and is comprised of all epitopes for a given pathogen species across all individuals in the cohort. Only pathogens with > 5 epitopes recognized across all children in each cohort are included to allow for at least minimal statistical power to test for differences. Sample sizes (i.e. number of epitopes included in each point) are denoted by the symbol shape, Wilcoxon matched-pairs signed rank test with fdr-adjustment p-values are denoted by color, and the fold-change in the geometric-mean EBS per pathogen is plotted along the y-axis. Wilcoxon signed rank test with Bonferroni correction was used to determine significant differences in the distributions of the fold-changes (for those pathogens that reached statistical significance) and are denoted by the asterisks (**** = $p < 0.0001$ after Bonferroni correction for multiple comparisons; ns = $p > 0.05$).

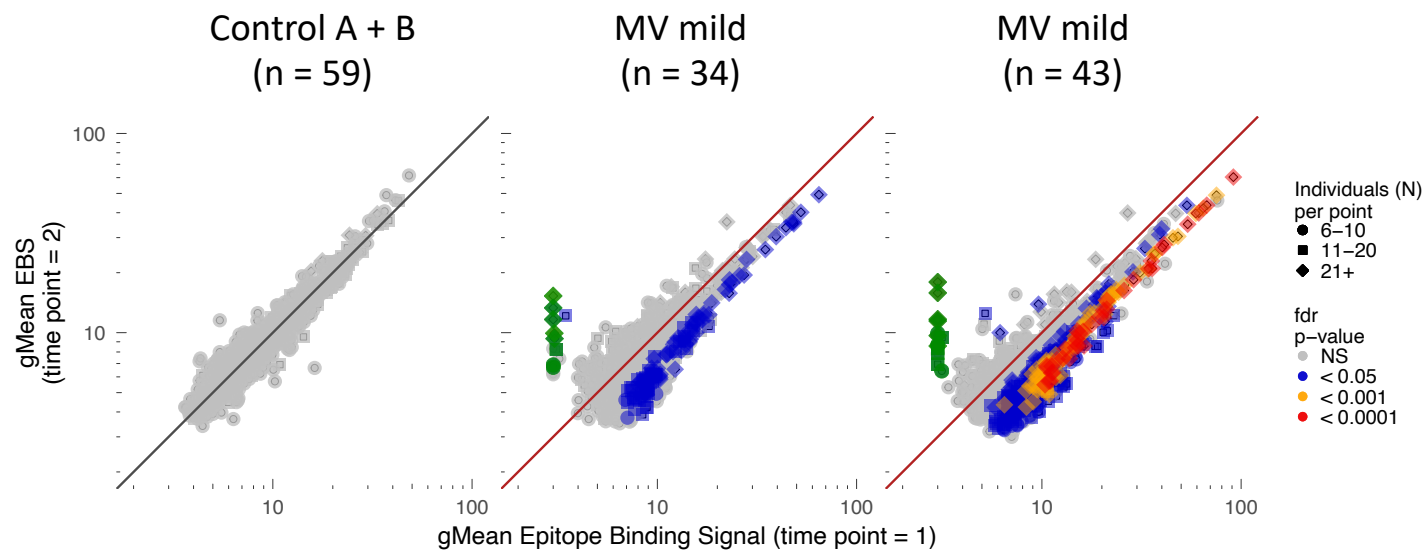


Figure S7. Cohort specific differences in detection of significantly changed epitopes is not due to sample size differences.

Achievement of statistical significance in any statistical test is inherently related to sample size. We checked to ensure that the cohort-specific differences noted in Figure 2D, namely the complete lack of detecting any statistically significant epitopes in the control cohorts, versus large numbers of significantly changed epitopes in the measles cohorts, was not due to the slightly smaller sample sizes among the control cohorts. To test this, we combined controls A and B to derive a cohort with a greater sample size (n = 53) than either of the two measles cohorts (n = 34 and n = 43). Still, we found no statistically significantly changed epitopes, ruling out both low sample sizes in the controls, or too large sample sizes (i.e. overpower) in the measles cohorts as a contributor to the observed differences between the controls and the measles infected individuals.

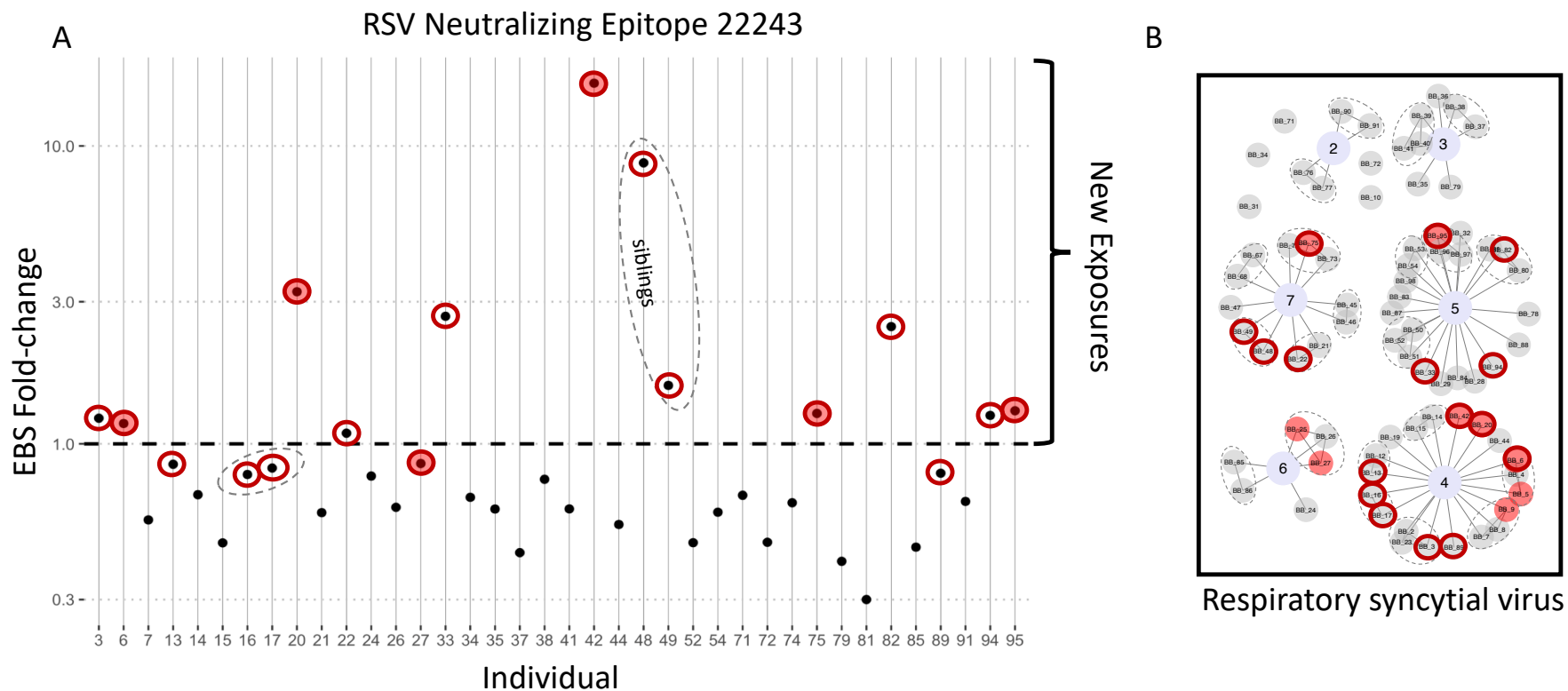


Figure S8. Measles depletes known neutralizing antibodies against RSV. (A) Fold-changes in the antibody epitope binding signal for the VirScan peptide Respiratory Syncytial Virus #2243 (TNSELLSLINDMPITNDQKKLMSNNVQIVRQQSYSIMSIKKEEVLAYVVQLPLYGV), which contains the 24-amino acid neutralizing epitope target of the RSV therapeutic mAbs: Palivizumab and Motavizumab.

There is evidence of new exposure to RSV during follow up based on either (i) the development of >3 new antibodies (not including #22243) to RSV during follow-up (red outlined circles) and/or (ii) increases in the mean EBS averaged across all RSV epitopes (except epitope 22243 in order to not bias these results here) recognized both before and after measles (shaded red points – as in Figure 4). For geographical reference of child location by Zip code, **(B)** here is adapted from figure 4 (see Figure 4 in the text for details).

Among children with no evidence of new exposures to RSV during follow-up, the mean fold-change in the epitope binding signal for epitope 22243 is 0.59 (SD 0.18). Thus, after measles and in the absence of evidence of new exposures, we detect a significant reduction in antibodies targeting a well known neutralizing RSV epitope that has been shown to protect children against RSV.

Of note, there is evidence of RSV transmission, particularly in district 4, based on a significantly increased odds (OR 4.5; $p = 0.007$) of having evidence of RSV (based on i and ii above) and being in district 4 versus other districts.

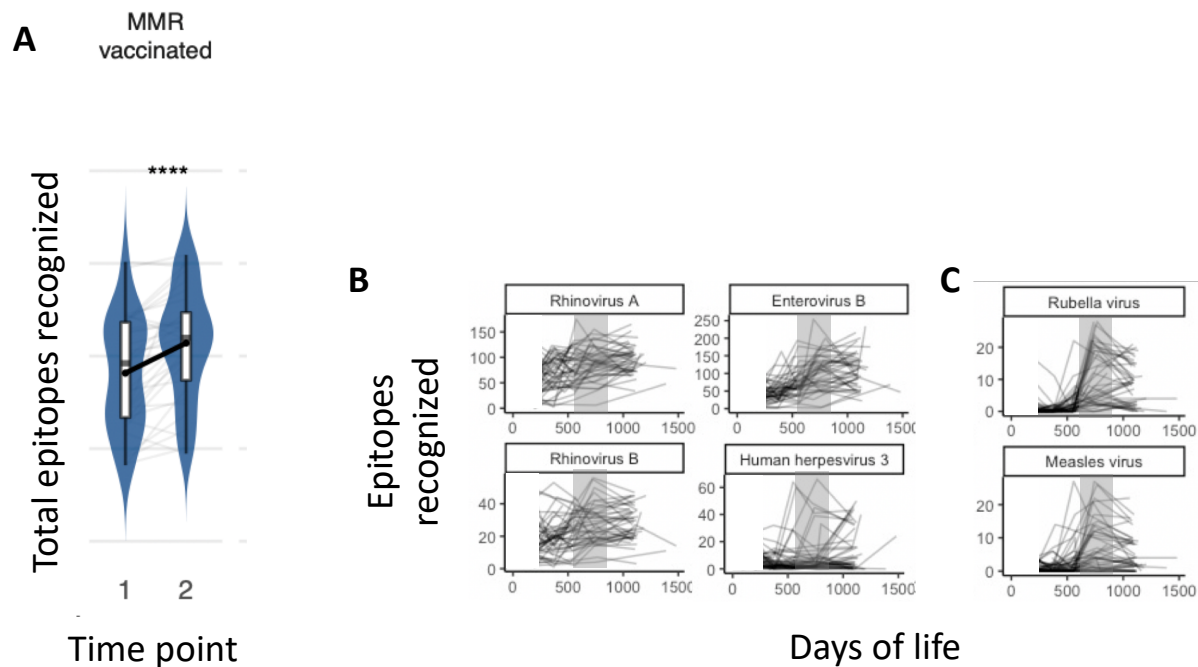
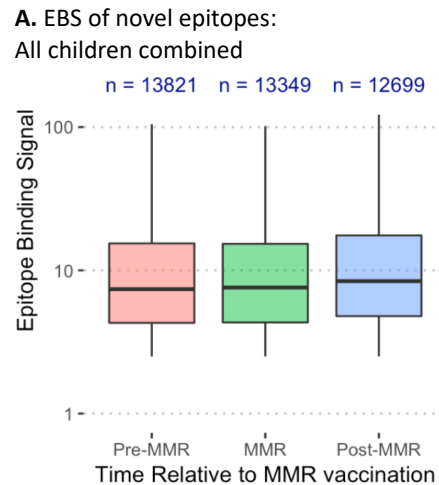


Figure S9. Increased epitope recognition following MMR vaccination is coincident but unrelated to MMR vaccination. The MMR vaccinated control cohort children are much younger (~1-2 years of age) than the other cohorts evaluated. At this early point in life, these individuals are building their immunological repertoire for the first time. Thus, the increase in epitopes recognized over the sampling interval (A, and shown in Figure 1A) is unrelated to the MMR vaccine, and is instead related to rapid exposures to new pathogens. Shown in (B), are the number of epitopes recognized at time points before, during and after the interval during which MMR was received. A consistently increasing slope of epitope recognition between 9 months and 3 years of life is observed for highly prevalent rhinoviruses and enteroviruses. Herpes Zoster (HHV-3) is also shown to increase in some individuals at different points during the 2+ years of follow up, likely representing individual exposures. The gray shaded regions indicate the time frame during which we detect using VirScan that most of the MMR vaccinated cohort received MMR vaccination – shown in (C) are coincident increases in both measles and rubella epitope recognition, representing vaccination with MMR.

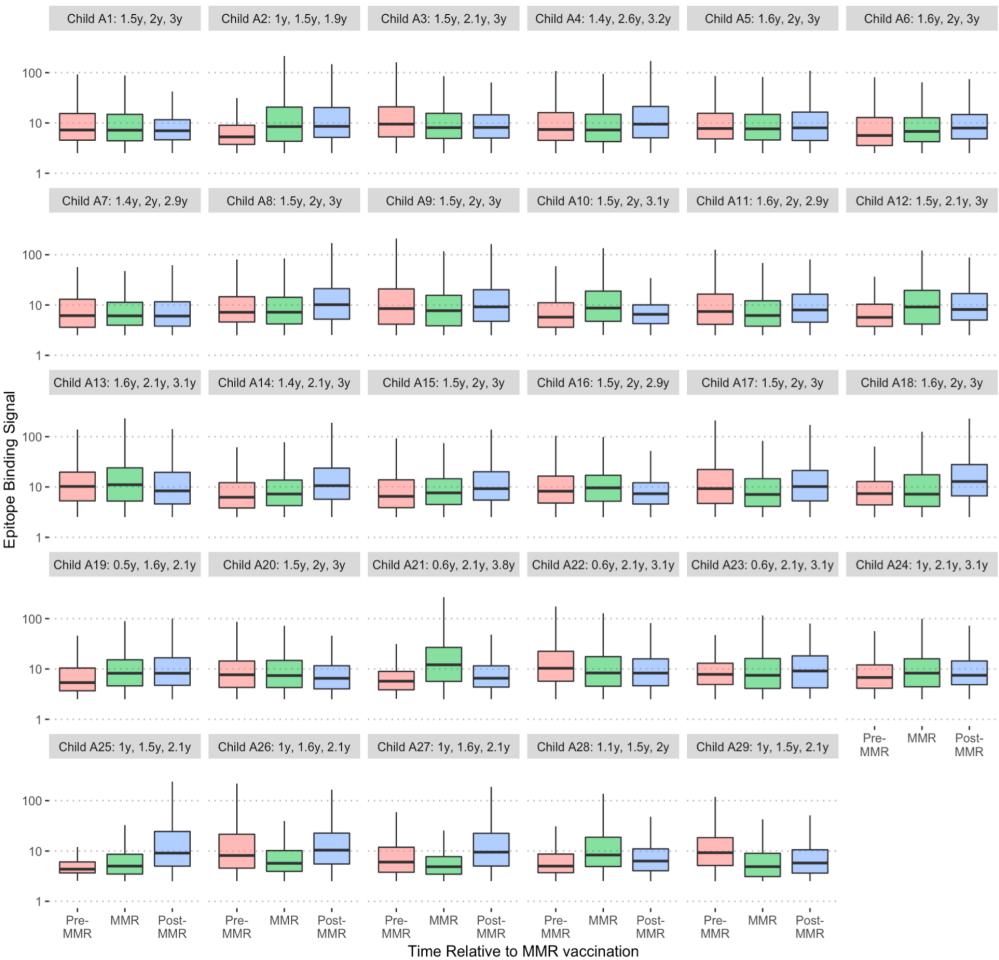
Figure S10. No effect of measles vaccination on ability to elicit antibody responses is observed. Epitope binding signals (EBS) of 'novel epitopes' (i.e. Antibody signal strength of epitopes that were detected for the first time in a child's life at each individual time point) were calculated in a birth cohort of children for the time points surrounding receipt of first measles vaccination: prior to first measles vaccination (pre-MMR), just following MMR (MMR), and the following time point (post-MMR).



Because antibodies to novel epitopes detected for the first time at the first sample after MMR (labeled "MMR") were due to exposures that occurred sometime between the pre-MMR and the MMR sample collections, these antibodies could have been elicited by exposures either before or after actual vaccine receipt. On the other hand, the pre-MMR and the post-MMR EBS values represent signal strength for antibodies that were elicited because of exposures that occurred either before or after vaccination, respectively.

Overall, we detect no differences in epitope binding signal strengths for epitopes recognized for the period before versus after MMR, suggesting that measles vaccination does not affect ability to elicit primary antibody responses. (A) shows all epitopes from all 29 children assessed and (B) shows EBS for each individual child. Values (n) shown in (A) represent the number of novel epitopes analyzed at each time point across 29 children and thus a similar number of novel epitopes are elicited at these early time points, indicating that children are continuing to be exposed to new pathogens. Additionally, the slight increase in EBS in the Post-MMR time point in (A), which are usually around 2-3 years, could be because these children are getting older and potentially have improved ability (compared to one year earlier, for example) to produce strong antibody responses in response to a pathogen exposure.

B. EBS of novel epitopes: Individual children: (age at each sample)



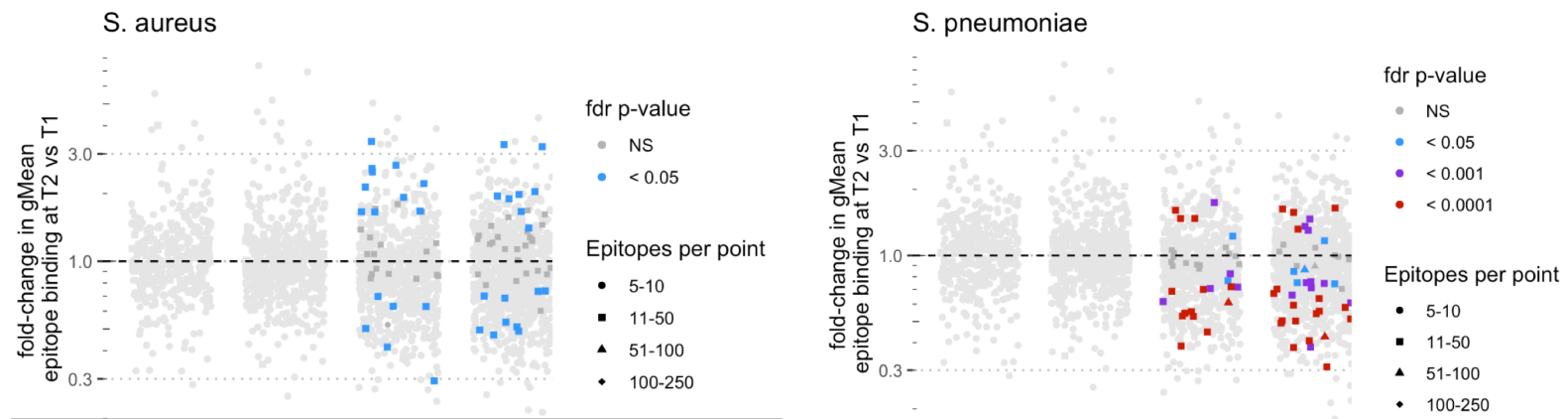


Figure S11. Distinct changes in antibody binding signals are observed for common colonizing ‘commensal-pathogen’ bacteria after measles.

Fold-changes in geometric mean antibody epitope binding signals (EBS) are shown for *S. aureus* and *S. pneumoniae*. Figures are as described in Fig 3A in the main text. Light gray (background) points represent all other pathogens, and are included for reference. Bacterial epitopes were not evaluated for the controls and are not shown. Compared to other pathogens, a relatively high proportion of significantly changed EBS for these commensal-pathogens is in a positive direction, potentially stemming from rapid bacterial acquisition or induction of bacterial replication during acute recovery following measles.

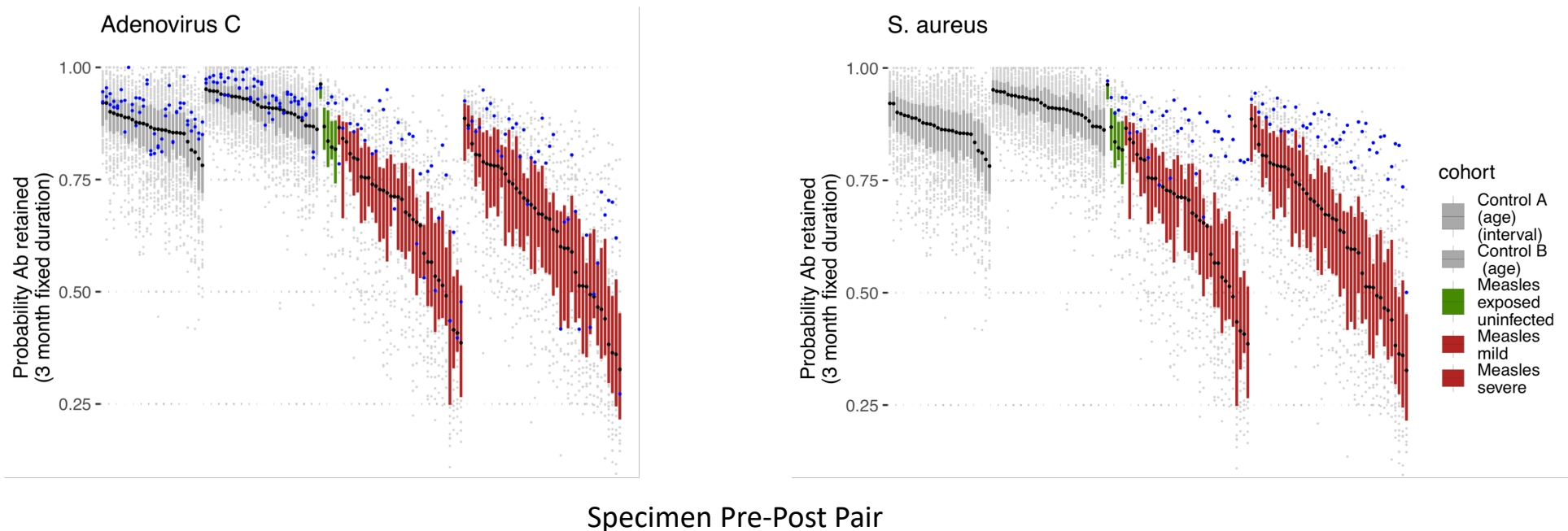


Figure S12. New exposures after measles lead to relatively high probabilities of antibody retention following measles.

In figure 1E, we observed increases in the number of epitopes recognized in certain children for adenovirus C and *S. aureus*. Here, looking at the same probabilities of epitope retention presented in Figure 2B, we find that for these pathogens, not only are the total numbers of epitopes recognized increased (as in Fig. 1E) but the relative probabilities of retaining epitopes (per individual) for these particular pathogens are also increased. For each plot below, the blue points represent the probability of retaining antibodies for adenovirus C (left panel) or *S. aureus* (right panel), overlaid over all other pathogens. Note the general distribution of blue points fall largely in the upper quartile of all of the pathogens evaluated.

In Figure 1D, we observed 39 individuals who had either no decrease, or had an increase in diversity of anti-adenovirus C antibodies. In all of these children, there were significant deletions in the specific adenovirus C repertoires detected before measles (shown below). However, since no change or even increased diversity was noted overall (Fig. 1E), this most likely represents new exposures (as evidenced in the next supplemental figure as well). In addition, in these children, the relative proportion of the anti-adenovirus C repertoire lost was low (relative to the effect of measles on the other pathogens). Together these data show that re-exposures following measles serves to rebuild the overall antibody repertoire for the particular pathogen.

References and Notes

1. A. Dabbagh, R. L. Laws, C. Steulet, L. Dumolard, M. N. Mulders, K. Kretsinger, J. P. Alexander, P. A. Rota, J. L. Goodson, Progress toward regional measles elimination — worldwide, 2000–2017. *MMWR Morb. Mortal. Wkly. Rep.* **67**, 1323–1329 (2018). [doi:10.15585/mmwr.mm6747a6](https://doi.org/10.15585/mmwr.mm6747a6) [Medline](#)
2. World Health Organization, New measles surveillance data for 2019 (2019); www.who.int/immunization/newsroom/measles-data-2019/en/.
3. A. Portnoy, M. Jit, M. Ferrari, M. Hanson, L. Brenzel, S. Verguet, Estimates of case-fatality ratios of measles in low-income and middle-income countries: A systematic review and modelling analysis. *Lancet Glob. Health* **7**, e472–e481 (2019). [doi:10.1016/S2214-109X\(18\)30537-0](https://doi.org/10.1016/S2214-109X(18)30537-0) [Medline](#)
4. H. S. Goodridge, S. S. Ahmed, N. Curtis, T. R. Kollmann, O. Levy, M. G. Netea, A. J. Pollard, R. van Crevel, C. B. Wilson, Harnessing the beneficial heterologous effects of vaccination. *Nat. Rev. Immunol.* **16**, 392–400 (2016). [doi:10.1038/nri.2016.43](https://doi.org/10.1038/nri.2016.43) [Medline](#)
5. C. Pirquet, Das Verhalten der kutanen Tuberkulinreaktion während der Masern. *Dtsch. Med. Wochenschr.* **34**, 1297–1300 (1908). [doi:10.1055/s-0028-1135624](https://doi.org/10.1055/s-0028-1135624)
6. D. E. Griffin, Measles virus-induced suppression of immune responses. *Immunol. Rev.* **236**, 176–189 (2010). [doi:10.1111/j.1600-065X.2010.00925.x](https://doi.org/10.1111/j.1600-065X.2010.00925.x) [Medline](#)
7. R. L. de Swart, M. Ludlow, L. de Witte, Y. Yanagi, G. van Amerongen, S. McQuaid, S. Yüksel, T. B. H. Geijtenbeek, W. P. Duprex, A. D. M. E. Osterhaus, Predominant infection of CD150⁺ lymphocytes and dendritic cells during measles virus infection of macaques. *PLOS Pathog.* **3**, e178 (2007). [doi:10.1371/journal.ppat.0030178](https://doi.org/10.1371/journal.ppat.0030178) [Medline](#)
8. H. Tatsuo, N. Ono, K. Tanaka, Y. Yanagi, SLAM (CDw150) is a cellular receptor for measles virus. *Nature* **406**, 893–897 (2000). [doi:10.1038/35022579](https://doi.org/10.1038/35022579) [Medline](#)
9. B. Hahm, N. Arbour, M. B. Oldstone, Measles virus interacts with human SLAM receptor on dendritic cells to cause immunosuppression. *Virology* **323**, 292–302 (2004). [doi:10.1016/j.virol.2004.03.011](https://doi.org/10.1016/j.virol.2004.03.011) [Medline](#)
10. R. D. de Vries, S. McQuaid, G. van Amerongen, S. Yüksel, R. J. Verburgh, A. D. M. E. Osterhaus, W. P. Duprex, R. L. de Swart, Measles immune suppression: Lessons from the macaque model. *PLOS Pathog.* **8**, e1002885 (2012). [doi:10.1371/journal.ppat.1002885](https://doi.org/10.1371/journal.ppat.1002885) [Medline](#)
11. J. De Salort, J. Sintes, L. Llinàs, J. Matesanz-Isabel, P. Engel, Expression of SLAM (CD150) cell-surface receptors on human B-cell subsets: From pro-B to plasma cells. *Immunol. Lett.* **134**, 129–136 (2011). [doi:10.1016/j.imlet.2010.09.021](https://doi.org/10.1016/j.imlet.2010.09.021) [Medline](#)
12. B. M. Laksono, C. Grosserichter-Wagener, R. D. de Vries, S. A. G. Langeveld, M. D. Brem, J. J. M. van Dongen, P. D. Katsikis, M. P. G. Koopmans, M. C. van Zelm, R. L. de Swart, *In vitro* measles virus infection of human lymphocyte subsets demonstrates high susceptibility and permissiveness of both naive and memory B cells. *J. Virol.* **92**, e00131-18 (2018). [doi:10.1128/JVI.00131-18](https://doi.org/10.1128/JVI.00131-18) [Medline](#)
13. J. J. Ryon, W. J. Moss, M. Monze, D. E. Griffin, Functional and phenotypic changes in

- circulating lymphocytes from hospitalized Zambian children with measles. *Clin. Diagn. Lab. Immunol.* **9**, 994–1003 (2002). [Medline](#)
14. V. G. Tamashiro, H. H. Perez, D. E. Griffin, Prospective study of the magnitude and duration of changes in tuberculin reactivity during uncomplicated and complicated measles. *Pediatr. Infect. Dis. J.* **6**, 451–453 (1987). [doi:10.1097/00006454-198705000-00007](https://doi.org/10.1097/00006454-198705000-00007) [Medline](#)
 15. M. J. Mina, C. J. E. Metcalf, R. L. de Swart, A. D. M. E. Osterhaus, B. T. Grenfell, Long-term measles-induced immunomodulation increases overall childhood infectious disease mortality. *Science* **348**, 694–699 (2015). [doi:10.1126/science.aaa3662](https://doi.org/10.1126/science.aaa3662) [Medline](#)
 16. R. D. de Vries, R. L. de Swart, Measles immune suppression: Functional impairment or numbers game? *PLOS Pathog.* **10**, e1004482 (2014). [doi:10.1371/journal.ppat.1004482](https://doi.org/10.1371/journal.ppat.1004482) [Medline](#)
 17. P. Isnard, T. Kula, V. Avettand Fenoel, D. Anglicheau, F. Terzi, C. Legendre, S. J. Elledge, G. Canaud, Temporal virus serological profiling of kidney graft recipients using VirScan. *Proc. Natl. Acad. Sci. U.S.A.* **116**, 10899–10904 (2019). [doi:10.1073/pnas.1821166116](https://doi.org/10.1073/pnas.1821166116) [Medline](#)
 18. J. L. Halliley, C. M. Tipton, J. Liesveld, A. F. Rosenberg, J. Darce, I. V. Gregoretti, L. Popova, D. Kaminiski, C. F. Fucile, I. Albizua, S. Kyu, K.-Y. Chiang, K. T. Bradley, R. Burack, M. Slifka, E. Hammarlund, H. Wu, L. Zhao, E. E. Walsh, A. R. Falsey, T. D. Randall, W. C. Cheung, I. Sanz, F. E.-H. Lee, Long-lived plasma cells are contained within the CD19⁺CD38^{hi}CD138⁺ subset in human bone marrow. *Immunity* **43**, 132–145 (2015). [doi:10.1016/j.immuni.2015.06.016](https://doi.org/10.1016/j.immuni.2015.06.016) [Medline](#)
 19. E. Hammarlund, A. Thomas, I. J. Amanna, L. A. Holden, O. D. Slayden, B. Park, L. Gao, M. K. Slifka, Plasma cell survival in the absence of B cell memory. *Nat. Commun.* **8**, 1781 (2017). [doi:10.1038/s41467-017-01901-w](https://doi.org/10.1038/s41467-017-01901-w) [Medline](#)
 20. I. J. Amanna, N. E. Carlson, M. K. Slifka, Duration of humoral immunity to common viral and vaccine antigens. *N. Engl. J. Med.* **357**, 1903–1915 (2007). [doi:10.1056/NEJMoa066092](https://doi.org/10.1056/NEJMoa066092) [Medline](#)
 21. M. D. Pescovitz, T. R. Torgerson, H. D. Ochs, E. Ocheltree, P. McGee, H. Krause-Steinrauf, J. M. Lachin, J. Canniff, C. Greenbaum, K. C. Herold, J. S. Skyler, A. Weinberg; Type 1 Diabetes TrialNet Study Group, Effect of rituximab on human in vivo antibody immune responses. *J. Allergy Clin. Immunol.* **128**, 1295–1302.e5 (2011). [doi:10.1016/j.jaci.2011.08.008](https://doi.org/10.1016/j.jaci.2011.08.008) [Medline](#)
 22. J. Hill, E. M. Krantz, K. A. Hay, S. Dasgupta, T. Stevens-Ayers, R. Bender Ignacio, M. Bar, J. Maalouf, S. Cherian, X. Chen, G. Pepper, S. R. Riddell, D. G. Maloney, M. Boeckh, C. J. Turtle, Durable preservation of antiviral antibodies after CD19 chimeric antigen receptor T cell immunotherapy. *Blood Adv.* 10.1182/bloodadvances.2019000717 (2019).
 23. K. Gadroen, C. N. Dodd, G. M. C. Masclee, M. A. J. de Ridder, D. Weibel, M. J. Mina, B. T. Grenfell, M. C. J. M. Sturkenboom, D. A. M. C. van de Vijver, R. L. de Swart, Impact and longevity of measles-associated immune suppression: A matched cohort study using data from the THIN general practice database in the UK. *BMJ Open* **8**, e021465 (2018). [doi:10.1136/bmjopen-2017-021465](https://doi.org/10.1136/bmjopen-2017-021465) [Medline](#)

24. B. M. Laksono, R. D. de Vries, R. J. Verburgh, E. G. Visser, A. de Jong, P. L. A. Fraaij, W. L. M. Ruijs, D. F. Nieuwenhuijse, H.-J. van den Ham, M. P. G. Koopmans, M. C. van Zelm, A. D. M. E. Osterhaus, R. L. de Swart, Studies into the mechanism of measles-associated immune suppression during a measles outbreak in the Netherlands. *Nat. Commun.* **9**, 4944 (2018). [doi:10.1038/s41467-018-07515-0](https://doi.org/10.1038/s41467-018-07515-0) [Medline](#)
25. G. J. Xu, T. Kula, Q. Xu, M. Z. Li, S. D. Vernon, T. Ndung'u, K. Ruxrungtham, J. Sanchez, C. Brander, R. T. Chung, K. C. O'Connor, B. Walker, H. B. Larman, S. J. Elledge, Comprehensive serological profiling of human populations using a synthetic human virome. *Science* **348**, aaa0698 (2015). [doi:10.1126/science.aaa0698](https://doi.org/10.1126/science.aaa0698) [Medline](#)
26. H. B. Larman, Z. Zhao, U. Laserson, M. Z. Li, A. Ciccia, M. A. Gakidis, G. M. Church, S. Kesari, E. M. Leproust, N. L. Solimini, S. J. Elledge, Autoantigen discovery with a synthetic human peptidome. *Nat. Biotechnol.* **29**, 535–541 (2011). [doi:10.1038/nbt.1856](https://doi.org/10.1038/nbt.1856) [Medline](#)
27. R. S. van Binnendijk, R. W. van der Heijden, G. van Amerongen, F. G. UytdeHaag, A. D. Osterhaus, Viral replication and development of specific immunity in macaques after infection with different measles virus strains. *J. Infect. Dis.* **170**, 443–448 (1994). [doi:10.1093/infdis/170.2.443](https://doi.org/10.1093/infdis/170.2.443) [Medline](#)
28. R. L. de Swart, R. D. de Vries, L. J. Rennick, G. van Amerongen, S. McQuaid, R. J. Verburgh, S. Yüksel, A. de Jong, K. Lemon, D. T. Nguyen, M. Ludlow, A. D. M. E. Osterhaus, W. P. Duprex, Needle-free delivery of measles virus vaccine to the lower respiratory tract of non-human primates elicits optimal immunity and protection. *NPJ Vaccines* **2**, 22 (2017). [doi:10.1038/s41541-017-0022-8](https://doi.org/10.1038/s41541-017-0022-8) [Medline](#)
29. M. M. Coughlin, A. S. Beck, B. Bankamp, P. A. Rota, Perspective on global measles epidemiology and control and the role of novel vaccination strategies. *Viruses* **9**, 11 (2017). [doi:10.3390/v9010011](https://doi.org/10.3390/v9010011) [Medline](#)
30. W. J. Moss, D. E. Griffin, Global measles elimination. *Nat. Rev. Microbiol.* **4**, 900–908 (2006). [doi:10.1038/nrmicro1550](https://doi.org/10.1038/nrmicro1550) [Medline](#)
31. M. J. Mina, J. A. McCullers, K. P. Klugman, Live attenuated influenza vaccine enhances colonization of *Streptococcus pneumoniae* and *Staphylococcus aureus* in mice. *mBio* **5**, e01040-13 (2014). [doi:10.1128/mBio.01040-13](https://doi.org/10.1128/mBio.01040-13) [Medline](#)
32. M. J. Mina, K. P. Klugman, The role of influenza in the severity and transmission of respiratory bacterial disease. *Lancet Respir. Med.* **2**, 750–763 (2014). [doi:10.1016/S2213-2600\(14\)70131-6](https://doi.org/10.1016/S2213-2600(14)70131-6) [Medline](#)
33. R. Cole, Part I. Etiology and clinical features of the pneumonia occurring in the hospital. *J. Am. Med. Assoc.* **70**, 1147–1153 (1918). [doi:10.1001/jama.1918.26010160003007a](https://doi.org/10.1001/jama.1918.26010160003007a)
34. A. N. Nelson, N. Putnam, D. Hauer, V. K. Baxter, R. J. Adams, D. E. Griffin, Evolution of T cell responses during measles virus infection and RNA clearance. *Sci. Rep.* **7**, 11474 (2017). [doi:10.1038/s41598-017-10965-z](https://doi.org/10.1038/s41598-017-10965-z) [Medline](#)
35. P. R. Hinton, J. M. Xiong, M. G. Johlfs, M. T. Tang, S. Keller, N. Tsurushita, An engineered human IgG1 antibody with longer serum half-life. *J. Immunol.* **176**, 346–356 (2006). [doi:10.4049/jimmunol.176.1.346](https://doi.org/10.4049/jimmunol.176.1.346) [Medline](#)

36. A. Dispenzieri, C. Tong, B. LaPlant, M. Q. Lacy, K. Laumann, D. Dingli, Y. Zhou, M. J. Federspiel, M. A. Gertz, S. Hayman, F. Buadi, M. O'Connor, V. J. Lowe, K.-W. Peng, S. J. Russell, Phase I trial of systemic administration of Edmonston strain of measles virus genetically engineered to express the sodium iodide symporter in patients with recurrent or refractory multiple myeloma. *Leukemia* **31**, 2791–2798 (2017). [doi:10.1038/leu.2017.120](https://doi.org/10.1038/leu.2017.120) [Medline](#)
37. D. E. Griffin, B. J. Ward, E. Jauregui, R. T. Johnson, A. Vaisberg, Immune activation in measles. *N. Engl. J. Med.* **320**, 1667–1672 (1989). [doi:10.1056/NEJM198906223202506](https://doi.org/10.1056/NEJM198906223202506) [Medline](#)
38. R. W. Blumberg, H. A. Cassady, Effect of measles on the nephrotic syndrome. *Am. J. Dis. Child.* **73**, 151–166 (1947). [doi:10.1001/archpedi.1947.02020370015003](https://doi.org/10.1001/archpedi.1947.02020370015003) [Medline](#)
39. M. K. Slifka, R. Antia, J. K. Whitmire, R. Ahmed, Humoral immunity due to long-lived plasma cells. *Immunity* **8**, 363–372 (1998). [doi:10.1016/S1074-7613\(00\)80541-5](https://doi.org/10.1016/S1074-7613(00)80541-5) [Medline](#)
40. M. J. Mina, B. T. Grenfell, C. J. E. Metcalf, Response to Comment on “Long-term measles-induced immunomodulation increases overall childhood infectious disease mortality”. *Science* **365**, eaax6498 (2019). [Medline](#)
41. World Health Organization, Measles fact sheet (2019); www.who.int/news-room/fact-sheets/detail/measles.
42. M. J. Mina, S. J. Elledge, Measles Immune Amnesia: Data and Code for Mina *et al.* *Science* 2019, Dryad (2019); <https://doi.org/10.5061/dryad.5tb2rbp0j>.
43. N. Mustonen, H. Siljander, A. Peet, V. Tillmann, T. Härkönen, J. Ilonen, H. Hyöty, M. Knip; DIABIMMUNE Study Group, Early childhood infections precede development of beta-cell autoimmunity and type 1 diabetes in children with HLA-conferred disease risk. *Pediatr. Diabetes* **19**, 293–299 (2018). [doi:10.1111/pedi.12547](https://doi.org/10.1111/pedi.12547) [Medline](#)
44. J. M. Norris, X. Yin, M. M. Lamb, K. Barriga, J. Seifert, M. Hoffman, H. D. Orton, A. E. Barón, M. Clare-Salzler, H. P. Chase, N. J. Szabo, H. Erlich, G. S. Eisenbarth, M. Rewers, Omega-3 polyunsaturated fatty acid intake and islet autoimmunity in children at increased risk for type 1 diabetes. *JAMA* **298**, 1420–1428 (2007). [doi:10.1001/jama.298.12.1420](https://doi.org/10.1001/jama.298.12.1420) [Medline](#)
45. R. Vita, S. Mahajan, J. A. Overton, S. K. Dhanda, S. Martini, J. R. Cantrell, D. K. Wheeler, A. Sette, B. Peters, The Immune Epitope Database (IEDB): 2018 update. *Nucleic Acids Res.* **47**, D339–D343 (2019). [doi:10.1093/nar/gky1006](https://doi.org/10.1093/nar/gky1006) [Medline](#)